# Bilayer systems of tantalum or zirconium nitrides and molybdenum for optimized diamond deposition

Angeline Poulon-Quintin, Cyril Faure, Lionel Teule-Gay, Jean-Pierre Manaud

▶ **To cite this version:**

Angeline Poulon-Quintin, Cyril Faure, Lionel Teule-Gay, Jean-Pierre Manaud. Bilayer systems of tantalum or zirconium nitrides and molybdenum for optimized diamond deposition. Thin Solid Films, 2010, 519 (5), pp.1600-1605. 10.1016/j.tsf.2010.08.011 . hal-00549358

**HAL Id: hal-00549358**
**https://hal.science/hal-00549358**

Submitted on 13 Jul 2022

**HAL** is a multi-disciplinary open access archive for the deposit and dissemination of scientific research documents, whether they are published or not. The documents may come from teaching and research institutions in France or abroad, or from public or private research centers.

L'archive ouverte pluridisciplinaire **HAL**, est destinée au dépôt et à la diffusion de documents scientifiques de niveau recherche, publiés ou non, émanant des établissements d'enseignement et de recherche français ou étrangers, des laboratoires publics ou privés.

# Bilayer systems of tantalum or zirconium nitrides and molybdenum for optimized diamond deposition

Angéline Poulon-Quintin *, Cyril Faure, Lionel Teulé-Gay, Jean-Pierre Manaud

*CNRS, Université de Bordeaux, ICMCB, Pessac, France*

A B S T R A C T

Thermo chemical computing validates the stability of different nitrides against Co, Mo, and methane up to 1150 K, showing the highest chemical stability against carburization for ZrN and TaN under static conditions.
Single zirconium and tantalum nitrides layers have been sputtered onto WC–Co substrates as diffusion barriers and buffer layers under specific reactive sputtering conditions. To improve the nuclei density of diamond during CVD processing, a thin Mo extra layer has been added (<500 nm). In this study, two bilayer systems have been tested: TaN–Mo and ZrN–Mo. Nano crystalline diamond has been grown under negative biased substrates. After diamond deposition, a massive carburization of molybdenum and tantalum nitride is observable whereas zirconium nitride is not. Nevertheless, a small amount of cobalt has migrated through the ZrN layer. The better efficiency of the ZrN layer to prevent diffusion of the Co element, leads to expect an increased adhesion of diamond on ZrN–Mo bilayer coating. A TEM study is done to improve understanding of phenomena occurring at the interfaces during process.

## 1. Introduction

Diamond films grown by Chemical Vapor Deposition (CVD) are widely used as surface overlay coating onto WC–Co cutting tools to improve their performances (endurance, surface hardness, thermal conductivity, friction, wear protection…). It is well known that the Co content has to be lower than 6 wt.% and the fraction of other carbides should be as small as possible to achieve satisfactory adhesion levels of CVD diamond films. The reduction of the Co content from the substrate causes toughness deterioration and reduces the tool lifetime. Whereas the reduction of the cemented carbide grain size (<1 μm) combined with an increase of the Co content (>10 wt.%) leads to mechanical properties close to those obtained with conventional grain size (>10 μm) and 3 wt.% Co content [1]. However the increase of the cemented carbide Co content is detrimental for the diamond adhesion. During deposition of $sp^3$ diamond film by CVD process onto sintered WC–Co substrates, formation of $sp^2$ graphitic species can occur because of the Co binder catalytic properties related to their valence electrons [2–4]. To improve the diamond adhesion with the substrate and the disagreements encountered, many pretreatment methods have been applied such as selective etching of Co [5–9], forming stable Co compounds [10–13], giving a suitable diffusion barrier layer on the substrates [14–20] or a tungsten-carbide gradient coating [21] etc. The latter three strategies aim at blocking the way through which elemental Co could reach the diamond WC–Co substrate interface. According to the phase diagram of Co–C system in the temperature range of 975–1275 K (typical diamond CVD temperature), carbon is soluble in Co up to 0.2–0.3 wt.%. During the initial stage of the CVD process, the WC–Co substrate is exposed to a hydrocarbon rich atmosphere and carbon species can diffuse into the bulk of the binder phase until the carbon solubility is exceeded. Once the carbon concentration at the substrate surface is sufficiently large to promote solid carbon condensation, the preferential formation of graphite layer is promoted by the presence of the binder. Moreover, as a further consequence of carbon solubility in the binder phase, diffusion of carbon from the deposited diamond into the metal binder can also occur. To suppress the interaction between Co and the deposited diamond film, an interlayer with low diffusion coefficients for C and Co has to be used. Moreover, an interlayer material with an intermediate thermal expansion coefficient between WC–Co and diamond could relieve the residual thermal stresses. Improvement in adhesion using various interlayers, ranging from amorphous carbon to metallic materials (Cu, Mo, Nb, Pt, Ti, Ta, W and Ag) and ceramics (SiC, $Si_3N_4$, TiC, TiN and WC) has already been reported [22].

In a previous paper [17], we have shown that refractory nitrides like ZrN, NbN and TaN can act as efficient Co diffusion barriers for CVD diamond deposition on WC–Co substrates containing 12 wt.% of cobalt. In this study, we propose to focus on bilayer systems composed of a Co diffusion barrier (TaN or ZrN) and a thin metallic layer to improve the diamond nucleation. Amorphous Si coating can act as a promoter for diamond nucleation thanks to its good carbide former properties [23]. Unfortunately, Si is not compatible with most of

* Corresponding author.
*E-mail address:* a.poulon@icmcb-bordeaux.cnrs.fr (A. Poulon-Quintin).

transition or refractory nitrides because the lowest chemical potential values of formed silicides lead to inescapable destruction of the barrier. In this study, molybdenum is used as another candidate to improve the nuclei density of diamond during CVD processing.

## 2. Experimental

### 2.1. Deposition of nitrides layers

The substrates were WC–Co 12 wt.% plates 16 × 16 mm² and 5 mm thick. Prior to deposition, WC–Co subtrates have been blasted with alumina micro particles under the same conditions (air flow absolute pressure : $2 \times 10^5$ Pa; distance 10 cm), then cleaned in acetone for 1 h in an ultrasonic bath and finished under propan-2-ol vapor for 1 min. The roughness $R_a$ measured (White light confocal profilometer VEECO) was lower than 500 nm.

Nitride layers were deposited by reactive magnetron sputtering using Zr, Ta and Mo targets. The sputtering plant was Plassys MP700 equipped with a 75 mm in diameter target. Targets used were disks of pure Ta (99.98%), Zr (99.8%) and Mo (99.98%) from Cerac. Ultra pure nitrogen (Dinal Alphagaz 2; >99.999%) was added as reactive gas to argon gas (Dinal Alphagaz 2) purified through a R.D. Mathis purifier (titanium getter at 1075 K). The ultimate pressure for all deposits was in the range of $2–3 \times 10^{-5}$ Pa. During deposit process, substrates were set on a heating plate with electronic temperature monitoring. The temperature of the substrates fixed at 673 K [17], was controlled with a thermocouple placed in contact with their surface. The distance between the target and the substrate surface was set on 70 mm for all depositions to assure a uniform thickness of deposited layers in respect of a fair deposition rate. Deposition rates were accurately extrapolated from nitrides layers thicknesses deposited on silicon wafers after phases identification by X-ray diffraction. The deposition parameters are presented in Table 1.

### 2.2. Diamond deposition

Diamond was deposited in a microwave enhanced plasma chemical vapor deposition reactor (silica tube crossing orthogonally the wave guide powered with a 1.2 kW) using a hydrogen–methane mixture. The total pressure was held at 40 hPa. Substrates were biased under −200 V. During the deposition time (6 h maximum), the partial pressure of methane was held at 0.4 hPa as described elsewhere [17]. The temperature of the sample surface was set at 1150 K (measured with a Raytek biband pyrometer).

### 2.3. Material characterization

X-ray diffraction was used to determine the deposited compounds. Experiments were carried out with a Philips PW1820 diffractometer with θ–2θ geometry and a Cu $K_\alpha$ radiation proportional detector. Morphology observations were carried out with a SEM Jeol JMS 6360A microscope equipped with a Jeol EDS system. TEM observations were carried out with a Jeol 2200FS equipped with a Jeol EDS and STEM system. Auger Electron Spectroscopy profiles were carried out with a VG Instrument microlab 310F. Etching was performed with an argon ion beam under 4 kV voltage and an ionic current of 0.5 mA. The spot surface was 3 μm² and the theoretical etching rate was 0.2 nm $s^{-1}$.

## 3. Results

### 3.1. Bilayer morphology before diamond growth

For Zr and Ta, binary phase diagrams show mainly the existence of two compounds $M_2N$ and MN with M Zr or Ta. Due to its lower enthalpy of formation $M_2N$ compounds should be preferentially synthesized under low temperature and pressure conditions. Thanks to the reactive magnetron sputtering process, the formation of the MN phase is possible when the partial pressure of nitrogen is increased. X-ray diffraction spectra (Fig. 1) show the presence of the hexagonal TaN (JCPDS 39-1484) and cubic ZrN (JCPDS 35-0753) compounds as well as the cubic Mo (JCPDS 03-065-7442) phase. TaN is obtained with 10% of nitrogen in sputtering gas whereas ZrN is obtained with only 6%. TaN layer is textured {110} and Mo layer {110}. ZrN layer is less textured with the presence of two main orientations {200} and {111}. AES in depth profiles (Fig. 2) show that after the bilayer deposit, no trace of Co is observable inside the diffusion layer. This result is in agreement with the thermochemical calculation from Thermodata Software [24]. No diffusion of Mo element inside the TaN or ZrN diffusion barriers is also noticeable even if the process occurs at 673 K. TEM observations of the TaN–Mo and ZrN–Mo bilayer coatings show that the materials deposited are very dense (Fig. 3). The morphology of the grains is more columnar for Mo and more of a structure of transition with fiber grains densely joined for TaN and ZrN layers. Average grain size width is 200 nm in diameter for Mo, 150 nm for TaN and 100 nm for ZrN with respectively a height of 0.4, 1.2 and 1 μm.

### 3.2. Thermochemical computation

Computing calculation with Thermodata Software has shown that for a temperature range of 1043 to 1143 K, a total pressure of 40 hPa and a partial pressure of 0.6 hPa of $CH_4$, the most stable nitrides against methane carburization are TaN and ZrN [17]. The stability of the nucleation layer under diamond deposition condition has been computed considering the enthalpy of formation of metallic element and all related carbides available in the data base for the following reaction:

$$xM_{(s)} + yCH_{4(g)} \rightarrow M_xC_{y(s)} + 2yH_{2(g)}.$$

Comparison between Mo, Nb and Ti has been done. Calculation results in static conditions at 1150 K for the expected reactions at the interface between the nucleation layer and the diffusion layer, are presented in Table 2. These three elements are good carbide formers as expected for a nucleation layer material. However, their stability with the materials selected for diffusion barriers varies. For titanium, nitridation can occur as consequence with possible reaction with TaN. When Ti is carburized, the same phenomenom might occur. Concerning Nb, the possibility to form $Nb_2C$ during carburization limits its used to ZrN diffusion barrier. Whereas the choice of Mo can be applied to both (TaN and ZrN) and seems to be a good candidate for the nucleation layer.

**Table 1**
Reactive sputtering deposition conditions of TaN, ZrN and Mo layers at 673 K.

| Sample | Total pressure (Pa) | Partial $N_2$ pressure (Pa) | $N_2$ percentage (%) | Power density (W $cm^{-2}$) | Target voltage (V) | Deposition rate (nm $min^{-1}$) | Layer thickness (μm) |
|---|---|---|---|---|---|---|---|
| TaN | 0.5 | 0.05 | 10 | 2.3 | −160 | 10.0 | 1 |
| ZrN | 0.5 | 0.03 | 6 | 4.0 | −280 | 16.5 | 1 |
| Mo | 0.5 | – | – | 2.3 | −190 | 20.0 | 0.2/0.4 |

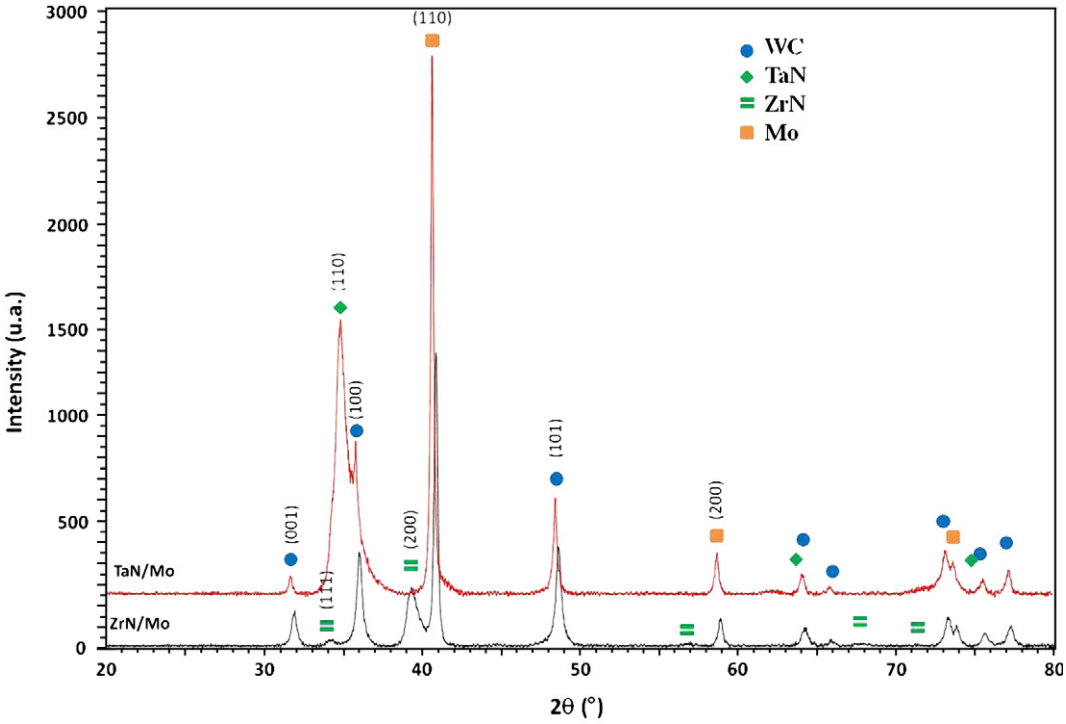


**Fig. 1.** X-ray diffraction patterns of TaN–Mo and ZrN–Mo bilayers deposited onto WC–Co substrates.

*3.3. Characterization of the bilayers after diamond deposition*

Diamond has been deposited at 1150 K on samples layered with TaN–Mo and ZrN–Mo. X-ray diffraction spectra (Fig. 4) show that ZrN layer has been preserved during diamond process whereas the hexagonal TaN is transformed into the cubic TaC phase (JCPDS 65-8264) less textured with the presence of four main orientations: {111}, {200}, {220} and {311}. For both diffusion layer types, Mo is carburized as witnessed by the presence of $Mo_2C$ (JCPDS 03-65-8766). Some small peaks seem to confirm the presence of Co after CVD process. However independently of the bilayer system observed, no molybdenum layer is still observable. On TEM pictures, the presence of TaC and ZrN layers is obvious but not for Mo layer. However close to the diffusion barrier where Mo layer would have been localized some circle grains are noticeable and dispersed into the diamond layer (Fig. 5). Based on EDS quantitative analyses and XRD results, these phases have been identified as $Co_6Mo_6C_2$ (JCPDS 80-6339) and $Co_2Mo_6C$ (JCPDS 89-4885) (Fig. 4). Raman analyses show that $sp^2$ graphite formation is not prevented whatever the bilayer system studied (Fig. 6) with amorphous $sp^2$ carbon species observable (result confirms by TEM diffraction study). Concerning the $sp^3$ species formed, presence of nano-grained diamond is established. The calculated ratio values between $sp^3$ and $sp^2$ species are similar (XPS quantification); respectively 0.8 for TaN–Mo and 0.9 for ZrN–Mo after 6 h of diamond deposit process. An estimation of the nucleation density after 3 h of diamond growth is $1.7\times10^6$ nucleus/cm² for TaN–Mo and $1.3\times10^6$ nucleus/cm² for ZrN–Mo.

## 4. Discussion

The results clearly demonstrate that as intermediate layers of Mo, TaN or ZrN on WC–Co substrates show different effects on subsequent diamond growth. Based on the comparison with results obtained without the Mo layer used on the top of TaN or ZrN intermediate layers, the diamond nucleation has been significantly promoted. For TaN and ZrN, the increase is time 20. The consequences on the adhesion of the diamond film have to be quantified. We have already showed [17] that an intermediate layer (TaN or ZrN) can effectively prevent the formation of detrimental graphite at film substrate interface thanks to their Co diffusion barrier properties. The low nucleation density of diamond observed and the diamond grain morphology (micrometric crystallites) have led to weak bonding

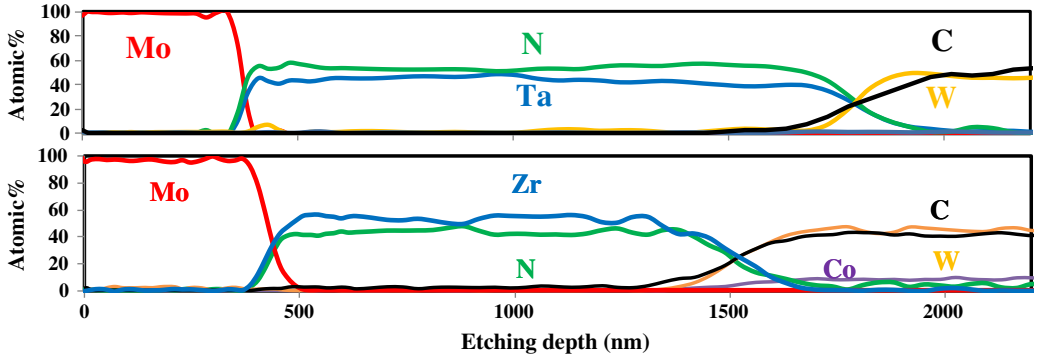


**Fig. 2.** AES in depth profiles of TaN–Mo and ZrN–Mo bilayers deposited onto WC–Co substrates.

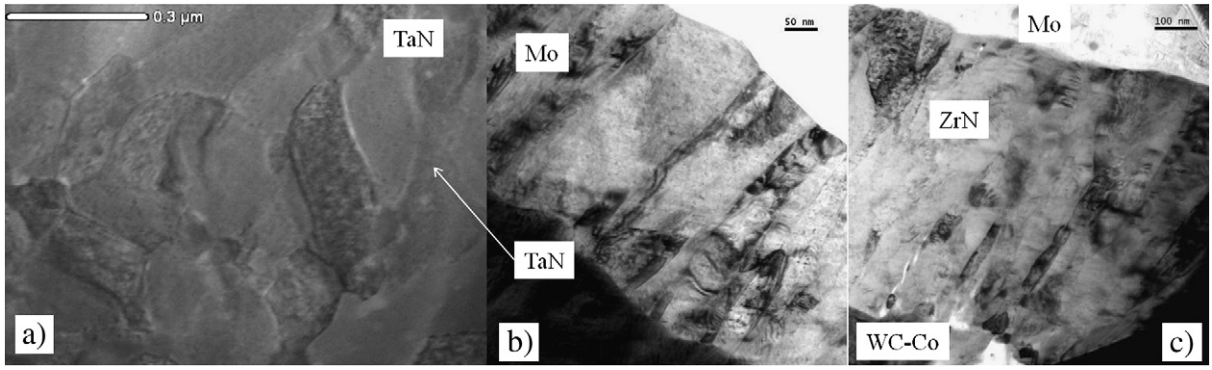


**Fig. 3.** TEM pictures (BF) of TaN–Mo and ZrN–Mo bilayers deposited onto WC–Co substrates. a) TaN fiber grain structure, b) Mo columnar grain structure, and c) ZrN fiber grain structure.

strength between diamond film and these interlayers. Whereas the use of bias during diamond deposition process has led to the formation of diamond nano-grains (NCD) as already be observed by other teams [25–27]. The Mo layer modification of morphology has also to be correlated with the use of a negative bias which leads to an ionic bombardment of the coated surface. Some authors have noticed modification of the surface roughness when they use Si wafer as substrate and the smoothing of edges [25]. They suppose that the polarization led to the formation of an ion flow deteriorating the plane faces increasing their roughness. These new defects are expected to be the new nucleation sites for diamond. They have shown the formation of NCD diamond. In our case, we need to decorrelate the beneficial effect of the Mo layer on nucleation from the bias effect. The printing effect (i.e. surface etching of the clusters) of the bias can explain the NCD diamond formation. However, the beneficial effect of Mo thin film on improved $sp^3$ formation can be related to the following two important factors.

First, as already observed with the use of Al nucleation layer coated on WC–Co substrate [28], Mo reacts with the binder phase Co during CVD process with the formation of $Co_6Mo_6C_2$ and $Co_2Mo_6C$ phases. Thereby this is supposed to decrease the graphite formation during CVD process. This function is especially important for diamond synthesis when Co binder is present even if a diffusion barrier such as TaN or ZrN is used. EDS-STEM study shows that whatever the diffusion barrier type (0.4 µm thickness both), Co can diffuse and is localized close to the top near surface inside diamond. With TaN–Mo bilayer system, after diamond CVD process, a lot of no-alloyed Co is observable (blue color on overlay view, Fig. 5). With ZrN–Mo bilayer system, after diamond CVD process, Co is alloyed with Mo and C (pink color on overlay view, Fig. 5) and few no-alloyed Co is observable. We can suppose than an optimization of the Mo thickness can be done to improve the efficiency of the TaN–Mo system and reduce the formation of graphite due to the Co binder close to the top interface with the consequence of the adhesion property degradation.

**Table 2**
Calculated values of free enthalpy for the phases susceptible to be formed during diamond process (Thermodata Software) at 1150 K.

| Interface | Chemical reaction | ΔrG°1150 K (kJ/mol) |
|---|---|---|
| TaN/Ti | $TaN + Ti \rightarrow Ta + TiN$ | −69.4 |
| TaN/TiC | $TaN + TiC \rightarrow TaC + TiN$ | −38.7 |
| ZrN/Ti | $ZrN + Ti \rightarrow Zr + TiN$ | 28.5 |
| ZrN/TiC | $ZrN + TiC \rightarrow ZrC + TiN$ | 13.3 |
| TaN/Nb | $TaN + Nb \rightarrow 1/2Ta_2N + 1/2Nb_2N$ | 6.3 |
| TaN/NbC | $TaN + NbC \rightarrow TaC + NbN$ | 28.0 |
| TaN/$Nb_2C$ | $TaN + 1/2Nb_2C \rightarrow 1/2Ta_2C + NbN$ | 23.8 |
| ZrN/Nb | $ZrN + 2Nb \rightarrow Zr + Nb_2N$ | 109.3 |
| ZrN/NbC | $ZrN + NbC \rightarrow ZrC + NbN$ | 66.9 |
| ZrN/$Nb_2C$ | $ZrN + NbC \rightarrow ZrC + 1/2Nb_2N + 1/4N_2$ | 103.6 |
| ZrN/Nb | $ZrN + 2Nb \rightarrow Zr + Nb_2N$ | 109.3 |
| TaN/Mo | $TaN + Mo \rightarrow 1/2Ta_2N + 1/2Mo_2N$ | 169.3 |
| TaN/MoC | $TaN + 2MoC \rightarrow TaC + Mo_2C + 1/2N_2$ | 22.6 |
| TaN/$Mo_2C$ | $TaN + Mo_2C \rightarrow TaC + Mo + 1/2N_2$ | 75.2 |
| ZrN/Mo | $ZrN + 2Mo \rightarrow Zr + Mo_2N$ | 435.3 |
| ZrN/MoC | $ZrN + 2MoC \rightarrow ZrC + Mo_2C + 1/2N_2$ | 61.5 |
| ZrN/$Mo_2C$ | $ZrN + Mo_2C \rightarrow ZrC + Mo + 1/2N_2$ | 114.1 |

Second, the fine-sized films have high surface energy and chemical reactivity. In this study, Mo layer still not exist and due to the CVD process conditions, Mo is localized inside circular grains close to the interface increasing the surface energy and chemical reactivity. At the initial stage of CVD process, the Mo grains are subjected to a carburization process and are transformed into carbide phase like $Mo_2C$. EDS-STEM analysis shows that for ZrN–Mo bilayer system, a significant quantity of Mo is not combined with Co as for TaN–Mo bilayer system. XRD spectrum confirms also the presence of a significant peak representative of the $Mo_2C$ phase for the ZrN–Mo bilayer system. These carbide particles can act as active sites for diamond nucleation producing a high nucleation density which should promote adhesion strength at diamond/substrate interface due to the increased contact area observable on TEM pictures (Fig. 5) and lowered interfacial voids [29,30]. Due to the high nucleation density promoted by the presence of Mo, nano-scaled diamond starts to nucleate at the early stage of process. This mechanism is confirmed by the experimental results obtained at different deposition periods (to be published). The formation of the carbide phase grains mixed with nano-scaled diamond grains close to the TaC or ZrN interfaces is comparable to a layer with a thickness around 2 µm. Such layer in contact with the outer-most diamond film can provide a stronger chemical bonding in comparison with the conventional mechanical interlocking as well as a continuous interface. Similar effects have been observed with other carbide metal formers employed as continue interlayers for diamond deposition such as Ti [31], Al [18] and Mo [32].

During the CVD process, formation of graphite or diamond necessitates a sufficiently large carbon concentration at the bilayer surface to promote solid carbon condensation. Both system studied consumes one part of carbon to carburize Mo and Mo–Co compounds. Methane carburization of these layers is a gas to solid reaction whose rate is expected to be determined by carbon diffusion into the near surface formed carbide. However due to the Mo nucleation layer, diamond nucleation and growth have started and nucleus can also act as localized sources of carbon. For TaN–Mo bilayer, diffusion of carbon from the deposited diamond (or graphite) and from the gas solid reaction occurs leading to the full carburization of TaN. Whereas for ZrN–Mo bilayer a supposed lower diffusion rate of carbon leads to the interlayer phase stability [17]. This mechanism modification combined with the presence of Mo can explain the difference of behavior of Co binder localization when compared to our previous study [17]. Previously using a single diffusion barrier layer, we have reported for TaN a very low Co diffusion compared to ZrN. We have

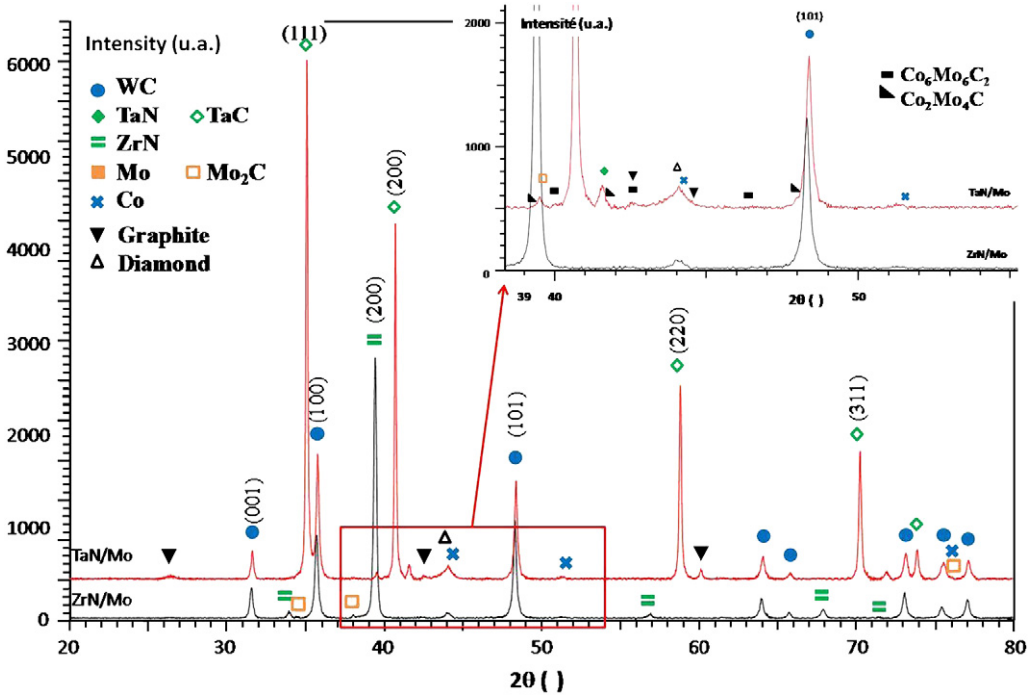


**Fig. 4.** X-ray diffraction patterns after diamond deposition process (6 h) onto TaN–Mo and ZrN–Mo bilayers deposited onto WC–Co substrates.

supposed that a progressive chemical transformation of the nitride into carbide from the surface to the interface instead a massive transformation, kept close to the interface the Co species without their diffusion to the surface where diamond nucleation occurs. The presence of Mo, its carburization and its affinity for Co (solid solution and binary compounds formation) as well as the carburization of the binary compounds formed may change the thermodynamic equilibrium of the system close to the interface with diamond. Moreover the efficiency of diamond nucleation thanks to Mo-phased grains combined with the effect of bias printing is supposed to increase the concentration of carbon reactive species close to the TaN top surface changing the velocity of the previously supposed progressive chemical transformation of the nitride into carbide from the surface to the interface. If now we suppose a massive transformation of TaN into TaC then Co species can diffuse to the surface where diamond nucleation occurs and partially reacts with the Mo–Co compounds. Co massive presence close to the TaC top surface is then explained. For the ZrN–Mo bilayer system, no significant modification of the mechanism is noticed excepted for the diamond nucleation phenomenon. Because XPS quantification of the ratio between $sp^3$ and $sp^2$ after 6 h of diamond deposit shows no significant differences between the two bilayer systems, we can suppose that only the adhesion would be affected due to the presence of the Co binder close to the interface for TaN–Mo bilayer with the consequence of an increase of the $sp^2$ graphite quantity at the interface.

## 5. Conclusion

The efficiency of the different bilayer systems (TaN–Mo and ZrN–Mo selected using thermochemical computation) with the aim to increase the diamond film growth has been investigated. TaN and ZrN thin film pre-coated on WC–Co substrates as Co diffusion barrier leads to a lower diamond nucleation density compared to the same system with a Mo top layer. After diamond deposition, a massive carburization of molybdenum and tantalum nitride is observable whereas zirconium nitride is not. Nevertheless, a small amount of cobalt has migrated through the ZrN layer and a more significant through the TaN layer. An optimization of the Mo layer thickness could be done to

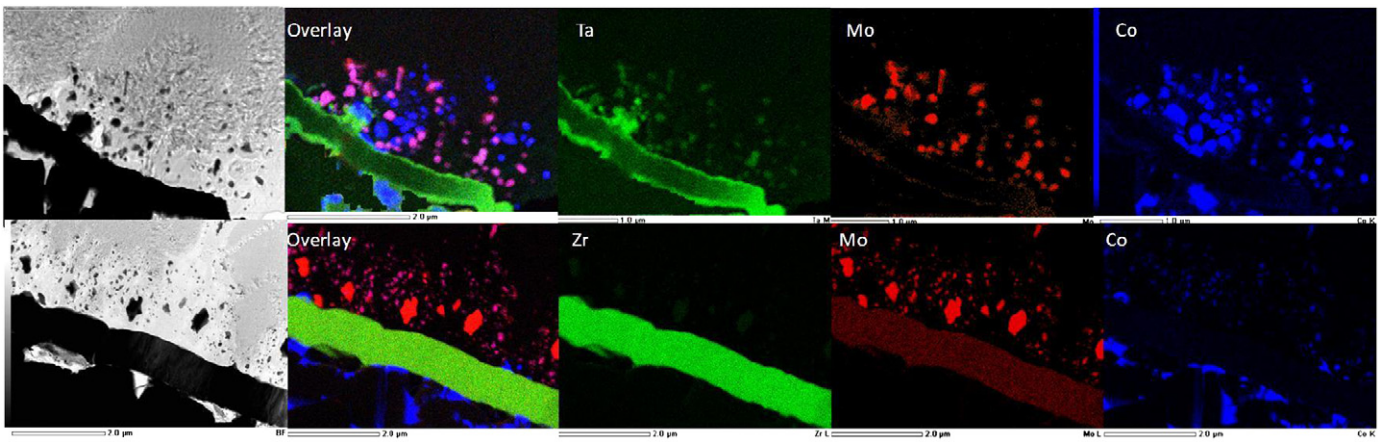


**Fig. 5.** TEM pictures and their corresponding EDS analysis of the multilayer materials after diamond deposition: TaN–Mo and ZrN–Mo systems.

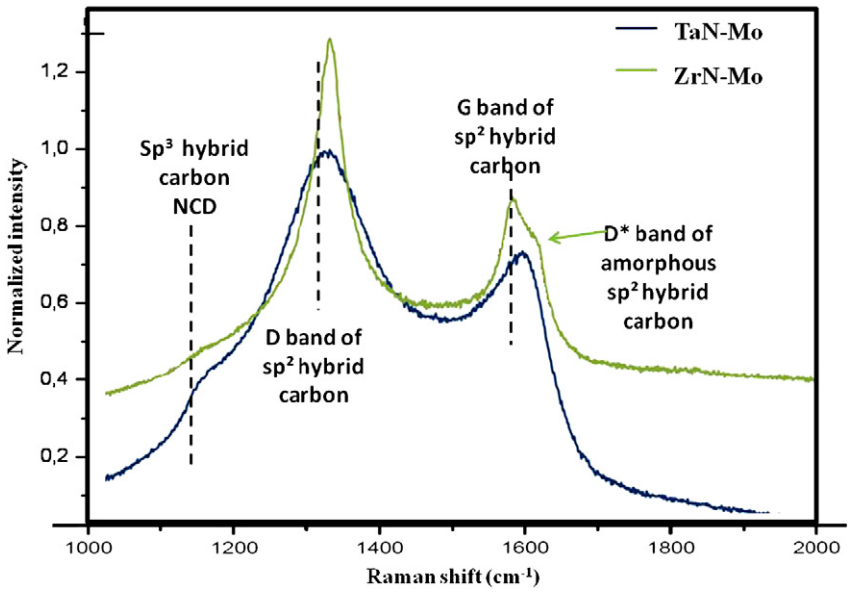


**Fig. 6.** Raman analyses of the multilayer materials after diamond deposition: TaN–Mo and ZrN–Mo systems.

reduce this phenomenon. The benefic effect of using a negative bias during CVD process to form nano-sized diamond is validated. The better efficiency of the ZrN layer to prevent diffusion of the Co element when a bilayer system is used, leads to expect an increased adhesion of diamond on ZrN–Mo bilayer coating.

## Acknowledgments

The author would like to thank “Le Conseil Regional d'Aquitaine” for its financial support, Dr. Michel Lahaye (CeCaMa, Université de Bordeaux1) for AES characterization and Dr. Christine Labrugère for XPS quantifications.

## References

[1] X.Y. Wu, W. Zhang, W. Wang, F. Yang, J.Y. Min, B.Q. Wang, J.D. Guo, J. Mater. Res. 19 (8) (2004) 2240.
[2] K. Mallika, R. Komanduri, Wear 224 (1999) 245.
[3] J.B. Donnet, D. Paulmier, H. Oulanti, T. Le Huu, Surf. Coat. Technol. 171 (2003) 41.
[4] S. Amirhaghi, H.S. Reehal, R.J.K. Wood, D.W. Wheeler, Surf. Coat. Technol. 135 (2001) 126.
[5] J.B. Donnet, D. Paulmier, H. Oulanti, T. LeHuu, Carbon 42 (2004) 2215.
[6] M.A. Neto, E. Pereira, Diamond Relat. Mater. 15 (2006) 465.
[7] V. Buck, F. Deuerler, H. Kluwe, B. Schmiler, Int. J. Refract. Met. H 20 (2002) 101.
[8] C.L. Geng, W.Z. Tang, L.F. Hei, S.T. Liu, F.X. Lu, Int. J. Refract. Met. H 25 (2007) 159.
[9] S.K. Sarangi, A. Chattopadhyay, A.K. Chattopadhyay, Appl. Surf. Sci. 254 (2008) 3721.
[10] A. Kopf, M. Sommer, R. Haubner, B. Lux, Diamond Relat. Mater. 10 (2001) 790.
[11] B. Sahoo, A.K. Chattopadhyay, Diamond Relat. Mater. 11 (2002) 1660.
[12] R. Polini, P. D'Antonio, S. Lo Casto, V.F. Ruisi, E. Traversa, Surf. Coat. Technol. 123 (2000) 78.
[13] W. Tang, Q. Wang, S. Wang, F. Lu, Diamond Relat. Mater. 9 (2000) 1744.
[14] W. Tang, Q. Wang, S. Wang, F. Lu, Surf. Coat. Technol. 153 (2002) 298.
[15] W. Tang, Q. Wang, S. Wang, F. Lu, Diamond Relat. Mater. 10 (2001) 1700.
[16] R. Polini, M. Barletta, Diamond Relat. Mater. 17 (2008) 325.
[17] J.P. Manaud, A. Poulon, S. Gomez, Y. Le Petitcorps, Surf. Coat. Technol. 202 (2007) 222.
[18] Y.S. Li, Y. Tang, Q. Yang, S. Shimada, R. Wei, K.Y. Lee, A. Hirose, Int. J. Refract. Met. H 26 (2008) 465.
[19] F. Huang, H.N. Xiao, Z.B. Ma, H.H. Wang, P.Z. Gao, Surf. Coat. Technol. 202 (2007) 180.
[20] Q.P. Wei, Z.M. Yu, L. Ma, D.F. Yin, J. Ye, Appl. Surf. Sci. 256 (5) (2009) 1322.
[21] I. Endler, A. Leonhardt, H.-J. Scheibe, R. Born, Diamond Relat. Mater. 5 (1996) 299.
[22] R. Polini, Thin Solid Films 515 (2006) 4.
[23] C.R. Lin, C.T. Kuo, R.M. Chang, Diamond Relat. Mater. 7 (1998) 1628.
[24] B. Cheynet, P.Y. Chevalier, E. Fischer, Calphad 26 (N°2) (2002) 167.
[25] W.L. Wang, G. Sánchez, M.C. Polo, R.Q. Zhang, J. Esteve, Appl. Phys. A 65 (1997) 241.
[26] M. Mojtahedzadeh Larijani, Thesis, Université Louis Pasteur de Strasbourg (2003).
[27] R. Stöckel, M. Stammler, K. Janischowsky, L. Ley, M. Albrecht, H.P. Strunk, J. Appl. Phys. 83 (1 January 1998).
[28] T. Kolber, A. Koepf, R. Haubner, H. Hutter, Int. J. Refract. Met. Hard Mater. 17 (1999) 445.
[29] Y.S. Li, A. Hirose, Chem. Phys. Lett. 433 (2006) 150.
[30] O. Ternyak, R. Akhvlediani, A. Hoffman, Diamond Relat. Mater. 14 (2005) 323.
[31] Y. Huang, H. Xiao, Z. Ma, J. Wang, P. Gao, Surf. Coat. Technol. 202 (2007) 180.
[32] Y.S. Huang, W. Qiu, C.P. Luo, Thin Solid Films 472 (2005) 20.